Phase transition properties of a ferroelectric spin-1/2 Ising superlattice



2001 J. Phys.: Condens. Matter 13 797

(http://iopscience.iop.org/0953-8984/13/5/302)

INSTITUTE OF PHYSICS PUBLISHING JOURNAL OF PHYSICS: CONDENSED MATTER

J. Phys.: Condens. Matter **13** (2001) 797–809 www.iop.org/Journals/cm PII: S0953-8984(01)15703-6

# Phase transition properties of a ferroelectric spin-1/2 Ising superlattice

**N El Aouad**[1], **B Laaboudi**[1], **M Kerouad**[1] **and M Saber**[1,2]

[1] Département de Physique, Faculté des Sciences, Université Moulay Ismail, BP 4010, Meknès, Morocco
[2] Dipartimento di Fisica, Universita di Padova, Via Marzolo 8, 35131 Padova, Italy

Received 21 July 2000, in final form 1 November 2000

**Abstract**

The phase transition properties of a ferroelectric superlattice described by the Ising model in a transverse field have been investigated using the effective-field theory with a probability distribution technique that accounts for the self-spin correlation functions. An independent interface plane has been assumed and the parameters that imitate $BaTiO_3/SrTiO_3$ structure have been used in our calculation. The Curie temperature, polarization, and dielectric constant have been obtained. The most striking feature is that the dielectric constant presents a maximum at room temperature. This kind of feature has been observed in a recent experimental measurement.

## 1. Introduction

During the past decade, there has been considerable interest in the study of ferroelectric films because they have received great attention in the research community and electronics industry [1–3]. Barium titanate $BaTiO_3$ is one of the most intensively investigated ferroelectrics since it was discovered in the 1940s [4]. Owing to its excellent dielectric, pyroelectric, and thermoelectric properties, $BaTiO_3$ has been widely used in the electronics industry in applications in capacitors, thermocouples, transducers, sensors, actuators [5, 6], etc. In recent years, with the modification of adding strontium, the $(Ba, Sr)TiO_3$ system for high-density memory has become one of the central focuses of ferroelectric film research and development activities, and the leading candidate for replacing $SiO_2$ in fabricating the new generation: extremely high-density DRAMs [7–9].

Ferroelectric superlattices have attracted significant attention recently because of a wide array of fascinating properties. The study of a magnetic superlattice that consists of two or more ferromagnets with different bulk properties has been motivated by the idea that the properties of the superlattice can be significantly different from those of its constituents. A detailed review of the properties of magnetic multilayers and superlattices has appeared [10].

Possibly because of the great difficulty of growing well characterized samples, few experimental studies of ferroelectric superlattices have been published, and those only in recent years. $(BaTiO_3)_2/(SrTiO_3)_2$ superlattices [11] and $(BaTiO_3)_5/(SrTiO_3)_5$ superlattices

0953-8984/01/050797+13$30.00  

[12] have been successfully prepared by molecular beam epitaxy. Dielectric measurements for $BaTiO_3/SrTiO_3$ superlattices have been carried out on a sample prepared by the pulsed laser deposition technique [13, 14]. Tabata *et al* [14] have shown that the dielectric properties of these superlattices exhibit considerably different behaviours from those of $BaTiO_3$ and $SrTiO_3$ single-phase films. The formation of dielectric and ferroelectric superlattices constitutes a promising approach for creating new super-ferroelectric materials and for study of the mechanism giving rise to ferroelectricity. A superlattice of $PbZrO_3/PbTiO_3$ has been fabricated by multi-ion-beam sputtering and its dielectric constant was obtained [15]. On the other hand, only a small amount of exploratory theoretical work has appeared [16–19]. Their starting point is the Landau free energy. Under the mean-field approximation, the dielectric properties of the same system have been studied [20–22]. The ferroelectric superlattice described by the Ising model in a transverse field has been studied recently using the effective-field theory [23–29].

Our aim in this paper is to extend previous work to study the properties of ferroelectric/paraelectric (FE/PE) superlattices. The system is described by the Ising model in a transverse field within the framework of the effective-field theory [30]. This technique is believed to give more exact results than the standard mean-field approximation. An independent interface plane has been assumed and parameters that imitate the $BaTiO_3/SrTiO_3$ structure have been used in our calculation. In the following section, we introduce the model and derive the equations that determine the plane longitudinal polarizations and the critical temperature of the superlattice as functions of temperature, exchange interactions, transverse field, and superlattice thickness. The phase diagrams, the polarizations, and the susceptibilities of the superlattice are discussed in section 3. Brief conclusions are given in section 4.

## 2. Model and formulation

We consider a superlattice consisting of two different ferroelectric materials, A and B, stacked alternately. For simplicity, we restrict our attention to the case of the simple cubic structure. The periodic condition suggests that we only have to consider one unit cell. A model of $(FE)_4/(PE)_4$ is depicted in figure 1, from which we can see that three of the four ferroelectric planes show bulk properties, i.e., with bulk exchange strength and transverse field, while one plane is an interface plane. Similarly, the four paraelectric planes consist of three planes with bulk paraelectric properties together with one interface plane. This model is different from the one used in the previous calculations [24, 26–29], which did not assume a separate interface plane between the two media. The existence of interface planes is intrinsic for perovskite ferroelectric superlattices [14]. The number of atomic planes in material A (B) is $L_a$ ($L_b$) and the thickness of the cell is $L = L_a + L_b$. The Hamiltonian of this system is given by

$$H = -\sum_{(i,j)} J_{ij}\sigma_i^z\sigma_j^z - \sum_i \Omega_i\sigma_i^x \tag{1}$$

where $\sigma_i^z$ and $\sigma_i^x$ denote the $z$- and $x$-components of a quantum spin $\vec{\sigma}_i$ of magnitude $\sigma = 1/2$ at site $i$. We consider only nearest-neighbour exchange, with $J_{ij} = J_{aa}$ for both spins in ferroelectric planes, $J_{ij} = J_{bb}$ for both spins in paraelectric planes, and $J_I$ for both spins in the interface planes and across the interface–ferroelectric or interface–paraelectric planes. We assume that $\Omega_i = \Omega_A$ in the ferroelectric planes, $\Omega_i = \Omega_B$ for a site in the paraelectric planes, and $\Omega_i = \Omega_I$ for the interface planes. The method that we use is the effective-field theory, described in [30, 31], which employs the probability distribution technique to account for the single-site spin correlations. Following this procedure, we find that

$$m_{i,z} = \langle\langle S_{iz}\rangle\rangle = \left\langle F\left(\sum_j J_{ij}S_{jz}, \Omega_i\right)\right\rangle \tag{2}$$

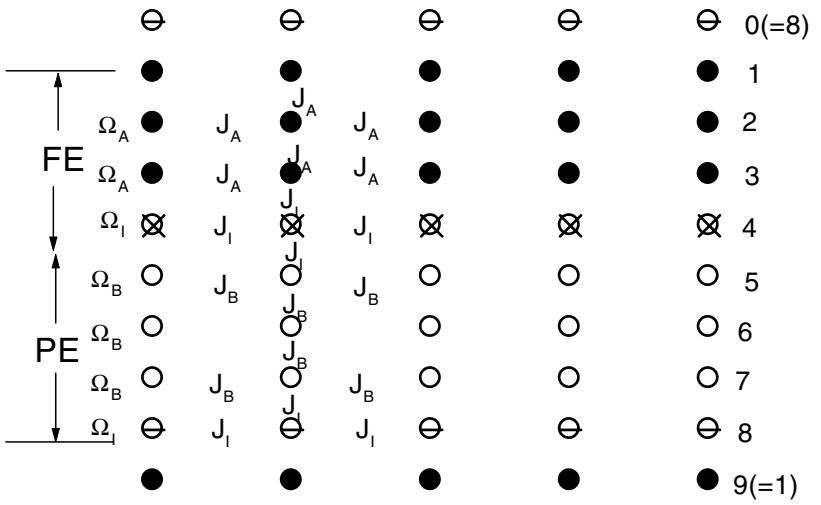


**Figure 1.** A schematic representation of a superlattice with four planes of ferroelectrics and four planes of paraelectrics.

where $m_{i,z}$ is the longitudinal polarization of the $i$th site. In the mean-field approximation, we would simply replace these spin operators by their thermal values $m_{n,z}$ (the longitudinal polarizations). However, it is at this point that a substantial improvement to the theory is made within the effective-field theory; we note that the spin operators have a finite set of basis states, so each of the averages over the function $F$ can be expressed as an average over a finite polynomial of spin operators belonging to the neighbouring spins. The details of the calculation can be found in [30, 31]. This leads to the plane longitudinal polarizations:

$$\begin{aligned} m_{n,z} = \frac{1}{2^{N+2N_0}} \sum_{i_1=0}^{N} \sum_{i_2=0}^{N_0} \sum_{i_3=0}^{N_0} C_{i_1}^{N} C_{i_2}^{N_0} C_{i_3}^{N_0} (1-2m_{n,z})^{i_1} (1+2m_{n,z})^{N-i_1} \\ \times (1-2m_{n-1,z})^{i_2} (1+2m_{n-1,z})^{N_0-i_2} (1-2m_{n+1,z})^{i_3} (1+2m_{n+1,z})^{N_0-i_3} \\ \times F\left[y_n, \Omega_n\right] \end{aligned} \tag{3}$$

where

$$y_n = \frac{1}{2}\left[J_{n,n}(N-2i_1) + J_{n,n-1}(N_0-2i_2) + J_{n,n+1}(N_0-2i_3)\right] \tag{4}$$

and

$$F(y,\Omega) = \frac{1}{2}\frac{y}{(y^2+\Omega^2)^{1/2}} \tanh\left[\frac{1}{2}\beta(y^2+\Omega^2)^{1/2}\right]. \tag{5}$$

We note that $m_{1,z}$ ($m_{L,z}$) is function of $m_{1,z}$ ($m_{L,z}$), $m_{2,z}$ ($m_{L-1,z}$), and $m_{L,z}$ ($m_{1,z}$). $N$ and $N_0$ are the numbers of nearest neighbours in the plane and between adjacent planes respectively ($N = 4$ and $N_0 = 1$ in the case of a simple cubic lattice), $C_K^l = l!/[k!(l-k)!]$, and $J_{i,j}$ in the definition of $y_n$ stands for one of the three exchange interactions ($J_{aa}$, $J_{bb}$, $J_I$) depending on where the spin pair is located. $\Omega_n$ stands for one of the three field strengths ($\Omega_A$, $\Omega_B$, $\Omega_I$) depending on where the spin is located. The periodic condition for the superlattice has to be satisfied, namely $m_{0,z} = m_{L,z}$ and $m_{L+1,z} = m_{1,z}$.

We have then obtained the self-consistent equations for the polarizations (equation (3)) that can be solved directly by numerical iteration. No further algebraic manipulation is necessary.

This is the advantage of introducing the probability distribution technique. The same equations hold for any arbitrary structure and, therefore, results for different structures can be obtained without carrying out the detailed algebra encountered when employing other techniques.

As we are interested in the calculation of the longitudinal ordering near the transition temperature, the usual argument that the plane longitudinal polarization $m_{n,z}$ tends to zero as the temperature approaches its critical value allows us to consider only terms linear in $m_{n,z}$ on approaching a critical temperature. Consequently, all terms of order higher than linear in equation (3) can be neglected. This leads to the calculation of the Curie temperature of the superlattice; all details of the formalism that we have used can be found in reference [26].

## 3. Results and discussion

In this paper, we denote respectively by $\sigma_{b,z}(\mathrm{A})$, $T_c^b(\mathrm{A})$, $\chi_{b,z}(\mathrm{A})$ the bulk longitudinal polarization, the bulk critical temperature and the bulk longitudinal susceptibility of a uniform lattice of material A which depend on $\Omega_\mathrm{A}$ and $J_{\mathrm{aa}}$. $\sigma_{b,z}(\mathrm{B})$ and $\chi_{b,z}(\mathrm{B})$ represent respectively the bulk longitudinal polarization and the bulk critical susceptibility of a uniform lattice of material B which depend on $\Omega_\mathrm{B}$ and $J_{\mathrm{bb}}$.

The values of the parameters are chosen as $J_{\mathrm{aa}} = 264$ K, $\Omega_\mathrm{A} = 0.01$ K for ferroelectric planes. These produce a bulk Curie temperature of 334.84 K. $J_{\mathrm{bb}} = 24$ K, $\Omega_\mathrm{B} = 87$ K. $J_\mathrm{I} = \sqrt{J_{\mathrm{aa}} J_{\mathrm{bb}}}$ and $\Omega_\mathrm{I} = \sqrt{\Omega_\mathrm{A}\Omega_\mathrm{B}}$ are defined as the exchange interaction and the transverse field in the interface planes. These parameters are chosen from references [22, 32].

### *3.1. Phase diagrams*

The period dependence of the Curie temperature of the superlattice is shown in figure 2. The plane number $n$ in the figure has different meanings for different curves. For curve a it stands for either the total number of ferroelectric planes or that of paraelectric planes, as the

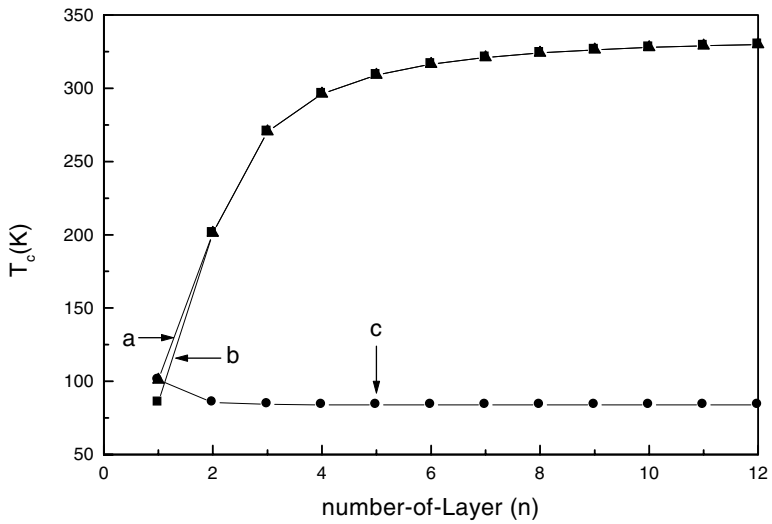


**Figure 2.** The period dependence of the Curie temperature $T_c$ (K). The number of planes $n$ stands for either the total number of ferroelectric planes or that of paraelectric planes. Curve a is for a superlattice of $(\mathrm{FE})_n/(\mathrm{PE})_n$, curve b is for a superlattice of $(\mathrm{FE})_n/(\mathrm{PE})_2$, and curve c is for a superlattice of $(\mathrm{FE})_1/(\mathrm{PE})_n$.

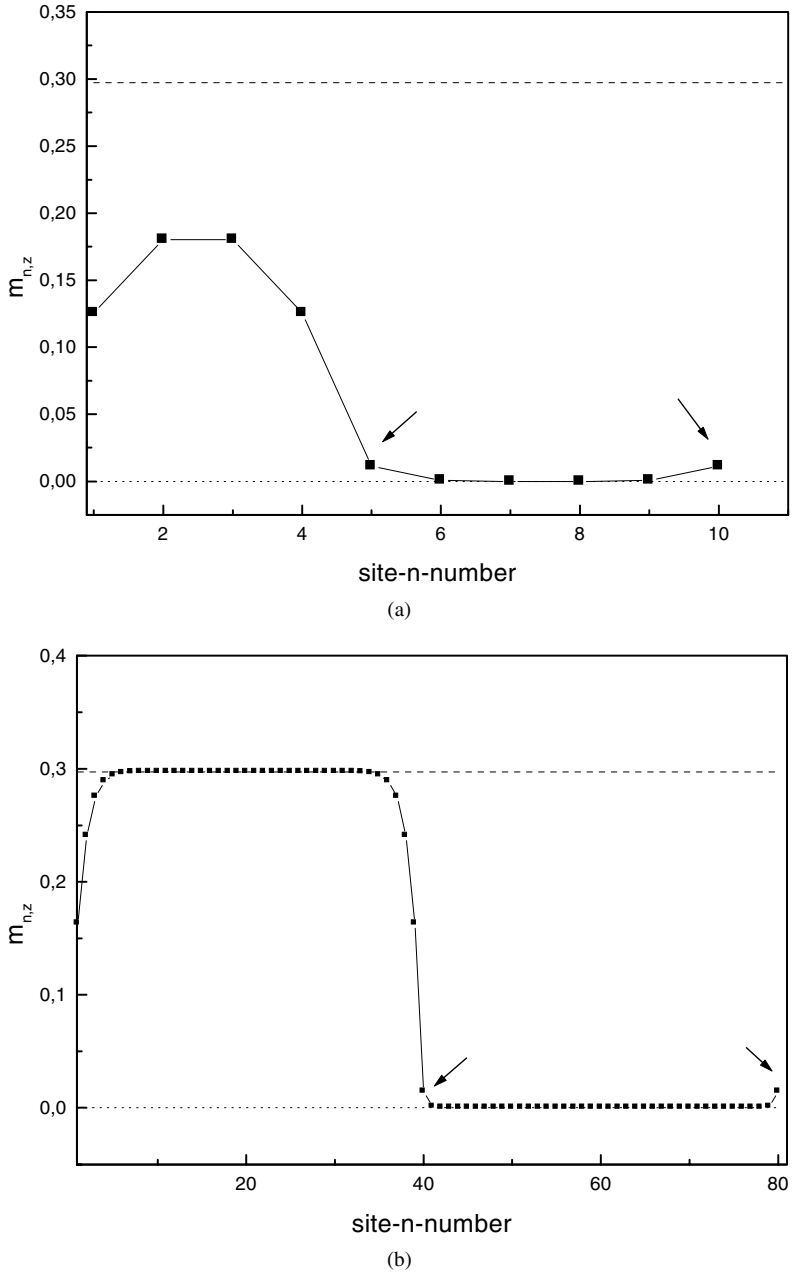


**Figure 3.** (a) Profiles of the polarization at room temperature for the superlattice $(FE)_5/(PE)_5$. The dashed and dotted horizontal lines correspond respectively to the bulk polarizations of materials A and B for the same parameters. (b) Profiles of the polarization at room temperature for the superlattice $(FE)_{40}/(PE)_{40}$. The dashed and dotted horizontal lines correspond respectively to the bulk polarizations of materials A and B for the same parameters.

curve represents the Curie temperature of a superlattice with equal thickness of the planes, i.e., $(FE)_n/(PE)_n$. Curve b stands for the Curie temperature of a superlattice $(FE)_n/(PE)_2$, where $n$ is the total number of ferroelectric planes. From these two curves we can see that

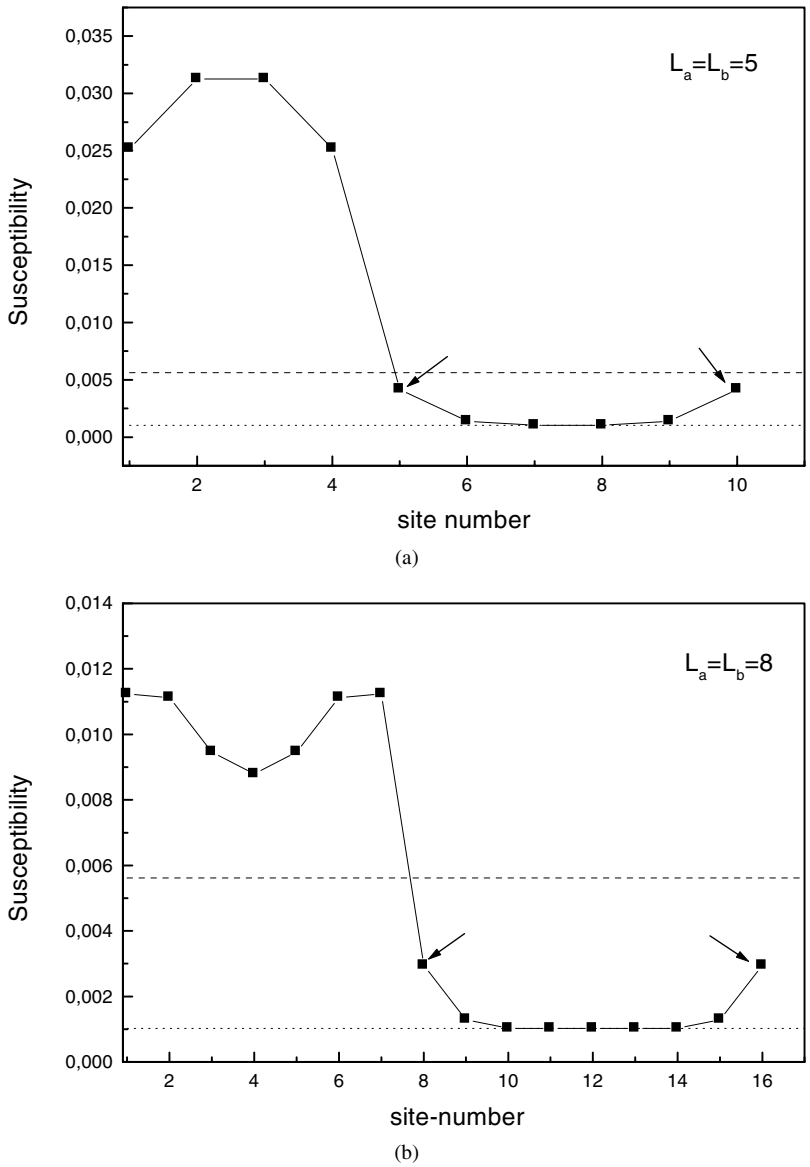


**Figure 4.** (a) Profiles of the susceptibility at room temperature for the superlattice $(FE)_5/(PE)_5$. The dashed and dotted horizontal lines correspond respectively to the bulk susceptibilities of materials A and B for the same parameters. (b) Profiles of the susceptibility at room temperature for the superlattice $(FE)_8/(PE)_8$. The dashed and dotted horizontal lines correspond respectively to the bulk susceptibilities of materials A and B for the same parameters. (c) Profiles of the susceptibility at room temperature for the superlattice $(FE)_{40}/(PE)_{40}$. The dashed and dotted horizontal lines correspond respectively to the bulk susceptibilities of materials A and B for the same parameters.

the Curie temperature increases with increasing number of ferroelectric planes and approaches the corresponding bulk ferroelectric Curie temperature when the period of the superlattice increases. The calculation has also been done for the $(FE)_n/(PE)_1$ superlattice and the results coincide with curve a. It is obvious that the Curie temperature depends upon the number of

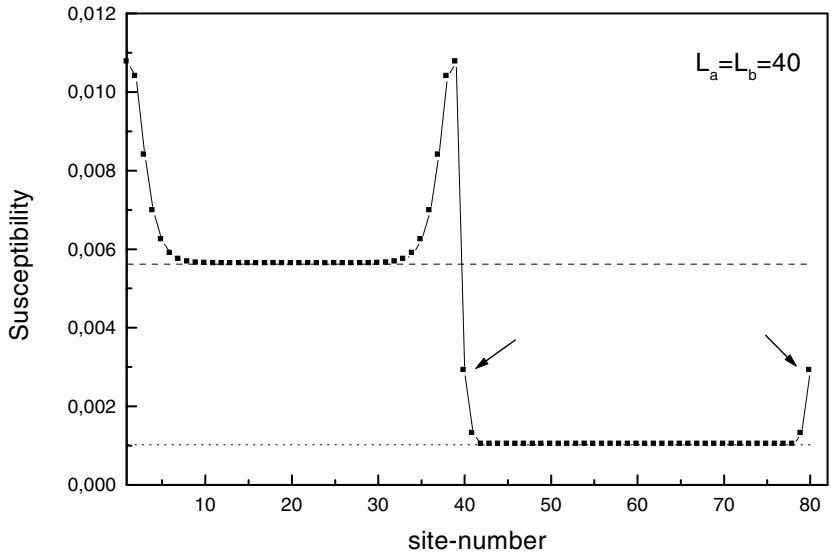


(c)

**Figure 4.** (Continued)

ferroelectric planes very strongly, and that the paraelectric plane plays a relatively weak role in the behaviour of the Curie temperature. To confirm this, we draw curve c, which represents the Curie temperature of the superlattice $(FE)_1/(PE)_n$. Here the number of ferroelectric planes is fixed to one, so the number of planes $n$ in the figure is the number of planes of paraelectrics. From this curve we find that the Curie temperature does not change with the thickness of the paraelectric planes except for the superlattice with one or two paraelectric planes.

### *3.2. Polarizations*

The profiles of the polarization at room temperature are shown in figure 3. The positions of the interface planes are marked by arrows. The dashed and dotted horizontal lines correspond respectively to the bulk polarizations of materials A and B for the same parameters. In figure 3(a) we show the profile of $(FE)_5/(PE)_5$. The polarization in the ferroelectric plane is reduced when compared with its bulk value, because the interface plane has a relative weak ferroelectricity. On the paraelectric side the polarization is virtually zero except at the interface plane. In this paraelectric plane the polarization is very weak and is induced by the interface plane. When we increase the period of the superlattice, as shown in figure 3(b) for a $(FE)_{40}/(PE)_{40}$ superlattice, the polarization on the ferroelectric side is the same as its bulk value at most sites, and is zero at sites away from the interface planes on the paraelectric side. However, around the interface plane, the polarization of the ferroelectric side is still much reduced, and is the same as in the case of a superlattice with a small period. The weak polarization of the interface plane and that of the nearest neighbours from either side are almost unchanged by the variation of the period.

### *3.3. Susceptibilities*

The magnetic properties are important in practice and, in particular, the longitudinal susceptibilities are interesting physical quantities which govern the characteristics of the

changes of the polarizations with the fields and can indicate phase transition properties, particularly the critical temperature. The phase transition is usually indicated by abnormal behaviour of the longitudinal susceptibility at the critical temperature. In order to obtain the longitudinal susceptibility, we apply a uniform longitudinal magnetic field $h$ across the superlattice, which adds to the Hamiltonian (1) a term

$$H_1 = -h \sum_{i=1}^{L} \sigma_{i,z} \tag{6}$$

describing the interaction of the longitudinal polarization with the magnetic field $h$. In order to calculate the magnetic longitudinal susceptibility, we apply the formalism of section 2. Equation (3) continues to apply, but the parameter $y_n$ is replaced by $y_n + h$. The longitudinal susceptibility of the $n$th plane is given by

$$\chi_{nz} = \left.\frac{\partial m_{n,z}}{\partial h}\right|_{h=0}. \tag{7}$$

The details of the calculations of the plane longitudinal susceptibilities are given in the appendix. To evaluate the longitudinal susceptibility of the superlattice, we follow the formalism of Wang *et al* [33]. As each plane can be treated as a capacitor, the capacitance of the superlattice is the sum of the capacitances of each of the planes connected in series. The total reciprocal permittivity is the sum of the reciprocal permittivities at each of the planes. Thus the total susceptibility (the superlattice longitudinal susceptibility) $\chi_z$ is determined from

$$(1 + \chi_z)^{-1} = \frac{1}{L} \sum_{n=1}^{L} (1 + \chi_{nz})^{-1} \tag{8}$$

where $L$ is the thickness of the unit cell.

The profiles of the susceptibility at room temperature are shown in figures 4(a), 4(b) and 4(c) respectively for $(FE)_5/(PE)_5$, $(FE)_8/(PE)_8$, and $(FE)_{40}/(PE)_{40}$. The dashed and dotted horizontal lines correspond to the bulk susceptibilities of materials A and B for the same parameters. The positions of the interface plane are indicated by arrows. The striking common feature is that the maximum value of the susceptibility appears at the plane on the ferroelectric side. For the $(FE)_5/(PE)_5$ superlattice in the ferroelectric phase, the susceptibility increases, passes through a maximum and decreases to reach the susceptibility in the interface (see figure 4(a)). This result is different from those published in reference [22], obtained using the mean-field approximation which is believed to give less exact results than ours obtained using the effective-field theory. For the two superlattices $(FE)_8/(PE)_8$ and $(FE)_{40}/(PE)_{40}$ (figures 4(b), 4(c)), in the ferroelectric phase, the susceptibility exhibits two maxima and tends asymptotically to $\chi_b$(A) away from the interface plane for the case $(FE)_{40}/(PE)_{40}$. In the paraelectric phase, the susceptibility always tends asymptotically to $\chi_b$(B) away from the interface plane (see figures 4(a), 4(b), and 4(c)). It is interesting to note that the difference between a superlattice with a small period and one with a large period is clearer in the ferroelectric plane. In the three cases, the susceptibility of the ferroelectric is much higher than that of the paraelectric side and even higher than its corresponding bulk value for $(FE)_5/(PE)_5$ and $(FE)_8/(PE)_8$. The susceptibility of the paraelectric side does not change much with the variation of the period and tends asymptotically to $\chi_b$(B) away from the interface. This indicates that the interface plane has a stronger influence on ferroelectric planes than on paraelectric planes.

The period dependence of the longitudinal susceptibility versus the number of planes in each sublattice ($L_a = L_b$) is shown in figure 5(a) (room temperature) and figure 5(b) ($T = 500$ K). Figure 5(a) shows that at room temperature, there is a peak around $(FE)_4/(PE)_4$.

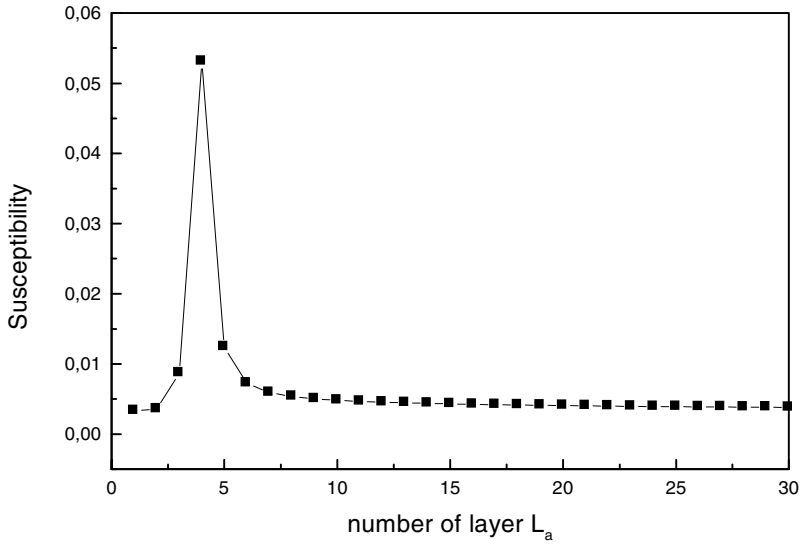


(a)

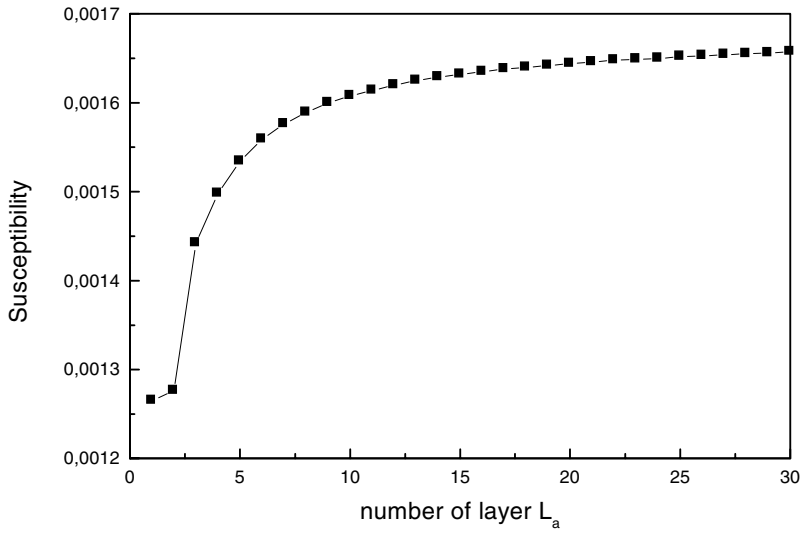


(b)

**Figure 5.** (a) The period dependence of the susceptibility at room temperature. (b) The period dependence of the susceptibility at $T = 500$ K.

This result has been observed experimentally for the $BaTiO_3/SrTiO_3$ superlattice recently [14]. Wang and Smith [22] have observed this peak around $(FE)_2/(PE)_2$; this disagreement with our results can be attributed to the fact that the authors used for their study the mean-field approximation. By recalling the Curie temperature from figure 2, we can easily find that the Curie temperature of $(FE)_4/(PE)_4$ is room temperature. This agreement between the behaviour of the susceptibility (figure 5(a)) and the phase diagram (figure 2) was not shown by Wang and Smith [22]. The peak position of the susceptibility will shift to a large period if the measurement is done at higher temperature. These trends were consistently obtained from

our calculations at different temperatures less than the bulk ferroelectric Curie temperature, but were not presented in the figures. It is well known that the susceptibilities of $BaTiO_3$ and $SrTiO_3$ increase with increasing film thickness [34–39]. Considering the behaviour of the susceptibility of the superlattice $BaTiO_3/SrTiO_3$, the structure of the system and the stress caused at the interface between the $BaTiO_3$ and $SrTiO_3$ planes, apparently, play an important role in the enhancement of the susceptibility. When the temperature is higher than the bulk ferroelectric Curie temperature, the susceptibility increases with the increase of the period; see figure 5(b).

## 4. Conclusions

We have studied the phase transition properties of a ferroelectric superlattice described by the Ising model in a transverse field using the effective-field theory with a probability distribution technique that accounts for the self-spin correlation functions. An independent interface plane has been assumed and the parameters that imitate the $BaTiO_3/SrTiO_3$ structure have been used in our calculation. We have found that the Curie temperature depends upon the number of ferroelectric planes very strongly, and that the paraelectric plane plays a relatively weak role in the behaviour of the Curie temperature. We have also shown that the dielectric properties of the superlattices are considerably different from those of $SrTiO_3$ and $BaTiO_3$ single-phase films. This indicates that the interface planes have a stronger influence on the superlattice and especially on the ferroelectric planes. Even though a lot of assumptions have been made in our calculations, the basic features observed experimentally have been reproduced from our model; there is a peak around $(FE)_4/(PE)_4$ in the curve of the period dependence of the susceptibility. Wang and Smith [22] have observed this peak around $(FE)_2/(PE)_2$; this disagreement with our results can be attributed to the fact that the authors used for their study the mean-field approximation.

The formation of dielectric and ferroelectric superlattices forms a promising approach for creating new super-ferroelectric materials and for the study of the mechanism giving rise to ferroelectricity.

## Acknowledgments

This work was completed during a visit of one of the authors (M Saber) to the Universita di Padova through the Programme of Research and Training in Italian Laboratories and the agreement between the CNRI (Italy) and the CNCPRST (Morocco). We thank both organizations.

## Appendix A. Calculation of the plane longitudinal susceptibilities

Taking into account the applied longitudinal magnetic field $h$, the plane longitudinal magnetizations take the forms

$$\begin{aligned} m_{1,z} = \frac{1}{2^{N+2N_0}} \sum_{i_1=0}^{N} \sum_{i_2=0}^{N_0} \sum_{i_3=0}^{N_0} & C_{i_1}^{N} C_{i_2}^{N_0} C_{i_3}^{N_0} (1-2m_{1,z})^{i_1} (1+2m_{1,z})^{N-i_1} (1-2m_{L,z})^{i_2} \\ & \times (1+2m_{L,z})^{N_0-i_2} (1-2m_{2,z})^{i_3} (1+2m_{2,z})^{N_0-i_3} \\ & \times F\left[\frac{1}{2}(J_{\mathrm{aa}}(N-2i_1) + J_{\mathrm{I}}(N_0-2i_2) + J_{\mathrm{aa}}(N_0-2i_3)) + h, \Omega_{\mathrm{A}}\right] \end{aligned} \tag{A.1}$$

$$m_{n,z} = \frac{1}{2^{N+2N_0}} \sum_{i_1=0}^{N} \sum_{i_2=0}^{N_0} \sum_{i_3=0}^{N_0} C_{i_1}^{N} C_{i_2}^{N_0} C_{i_3}^{N_0} (1-2m_{n,z})^{i_1} (1+2m_{n,z})^{N-i_1} \times (1-2m_{n-1,z})^{i_2} (1+2m_{n-1,z})^{N_0-i_2} (1-2m_{n+1,z})^{i_3} (1+2m_{n+1,z})^{N_0-i_3} \times F\left[y_n + h, \Omega_n\right] \tag{A.2}$$

$$m_{L,z} = \frac{1}{2^{N+2N_0}} \sum_{i_1=0}^{N} \sum_{i_2=0}^{N_0} \sum_{i_3=0}^{N_0} C_{i_1}^{N} C_{i_2}^{N_0} C_{i_3}^{N_0} (1-2m_{L,z})^{i_1} (1+2m_{L,z})^{N-i_1} \times (1-2m_{1,z})^{i_2} (1+2m_{1,z})^{N_0-i_2} (1-2m_{L-1,z})^{i_3} (1+2m_{L-1,z})^{N_0-i_3} \times F\left[\frac{1}{2}(J_{\mathrm{I}}(N-2i_1) + J_{\mathrm{I}}(N_0-2i_2) + J_{\mathrm{I}}(N_0-2i_3)) + h, \Omega_{\mathrm{I}}\right] \tag{A.3}$$

where

$$y_n = \frac{1}{2}\left[J_{n,n}(N-2i_1) + J_{n,n-1}(N_0-2i_2) + J_{n,n+1}(N_0-2i_3)\right]. \tag{A.4}$$

By differentiating the equations of the plane longitudinal magnetizations (equations (A.1)–(A.3)) with respect to $h$ and taking the limit when $h$ goes to zero, we get the following set of equations:

$$\left.\frac{\partial m_{1,z}}{\partial h}\right|_{h=0} = A_{1,1}\left.\frac{\partial m_{1,z}}{\partial h}\right|_{h=0} + A_{1,2}\left.\frac{\partial m_{2,z}}{\partial h}\right|_{h=0} + A_{1,L}\left.\frac{\partial m_{L,z}}{\partial h}\right|_{h=0} + B_1 \tag{A.5}$$

$$\left.\frac{\partial m_{n,z}}{\partial h}\right|_{h=0} = A_{n,n-1}\left.\frac{\partial m_{n-1,z}}{\partial h}\right|_{h=0} + A_{n,n}\left.\frac{\partial m_{n,z}}{\partial h}\right|_{h=0} + A_{n,n+1}\left.\frac{\partial m_{n+1,z}}{\partial h}\right|_{h=0} + B_n \tag{A.6}$$

$$\left.\frac{\partial m_{L,z}}{\partial h}\right|_{h=0} = A_{L,L-1}\left.\frac{\partial m_{L-1,z}}{\partial h}\right|_{h=0} + A_{L,L}\left.\frac{\partial m_{L,z}}{\partial h}\right|_{h=0} + A_{L,1}\left.\frac{\partial m_{1,z}}{\partial h}\right|_{h=0} + B_L. \tag{A.7}$$

The sets of equations (A.5)–(A.7) yield

$$C_{n,n-1}\chi_{n-1,z} + C_{n,n}\chi_{n,z} + C_{n,n+1}\chi_{n+1,z} = B_n \qquad \text{for } 1 \leqslant n \leqslant L \tag{A.8}$$

with

$$\begin{aligned} C_{n,n-1} &= -A_{n,n-1} \\ C_{n,n} &= 1 - A_{n,n-1} \\ C_{n,n+1} &= -A_{n,n+1}. \end{aligned} \tag{A.9}$$

Equation (A.8) is a set of $L$ equations from which the plane longitudinal susceptibilities are obtained. The expressions for the coefficients are

$$A_{n,n-1} = \frac{1}{2^{N+2N_0}} \sum_{i_1=0}^{N} \sum_{i_2=0}^{N_0} \sum_{i_3=0}^{N_0} \sum_{i=0}^{i_2} \sum_{j=0}^{N_0-i_2} C_{i_1}^{N} C_{i_2}^{N_0} C_{i_3}^{N_0} C_i^{i_2} C_j^{N_0-i_2} (-1)^i 2^{i+j} (i+j) \times (m_{n-1,z})^{i+j-1} (1-2m_{n,z})^{i_1} (1+2m_{n,z})^{N-i_1} (1-2m_{n+1,z})^{i_3} \times (1+2m_{n+1,z})^{N_0-i_3} F\left[y_n, \Omega_n\right] \tag{A.10}$$

$$A_{n,n} = \frac{1}{2^{N+2N_0}} \sum_{i_1=0}^{N} \sum_{i_2=0}^{N_0} \sum_{i_3=0}^{N_0} \sum_{i=0}^{i_1} \sum_{j=0}^{N-i_1} C_{i_1}^{N} C_{i_2}^{N_0} C_{i_3}^{N_0} C_i^{i_1} C_j^{N-i_1} (-1)^i 2^{i+j} (i+j) \times (m_{n,z})^{i+j-1} (1-2m_{n-1,z})^{i_2} (1+2m_{n-1,z})^{N_0-i_2} (1-2m_{n+1,z})^{i_3} \times (1+2m_{n+1,z})^{N_0-i_3} F\left[y_n, \Omega_n\right] \tag{A.11}$$

$$A_{n,n+1} = \frac{1}{2^{N+2N_0}} \sum_{i_1=0}^{N} \sum_{i_2=0}^{N_0} \sum_{i_3=0}^{N_0} \sum_{i=0}^{i_3} \sum_{j=0}^{N_0-i_3} C_{i_1}^{N} C_{i_2}^{N_0} C_{i_3}^{N_0} C_{i}^{i_3} C_{j}^{N_0-i_3} (-1)^i 2^{i+j} (i+j) (m_{n+1,z})^{i+j-1}$$
$$\times (1-2m_{n,z})^{i_1} (1+2m_{n,z})^{N-i_1} (1-2m_{n-1,z})^{i_2} (1+2m_{n-1,z})^{N_0-i_2}$$
$$\times F\,[y_n, \Omega_n] \tag{A.12}$$

$$B_1 = \frac{1}{2^{N+2N_0}} \sum_{i_1=0}^{N} \sum_{i_2=0}^{N_0} \sum_{i_3=0}^{N_0} C_{i_1}^{N} C_{i_2}^{N_0} C_{i_3}^{N_0} (1-2m_{1,z})^{i_1} (1+2m_{1,z})^{N-i_1} (1-2m_{L,z})^{i_2}$$
$$\times (1+2m_{L,z})^{N_0-i_2} (1-2m_{2,z})^{i_3} (1+2m_{2,z})^{N_0-i_3}$$
$$\times g\left[\frac{1}{2}(J_{\mathrm{aa}}(N-2i_1) + J_{\mathrm{I}}(N_0-2i_2) + J_{\mathrm{aa}}(N_0-2i_3)), \Omega_{\mathrm{A}}\right] \tag{A.13}$$

$$B_n = \frac{1}{2^{N+2N_0}} \sum_{i_1=0}^{N} \sum_{i_2=0}^{N_0} \sum_{i_3=0}^{N_0} C_{i_1}^{N} C_{i_2}^{N_0} C_{i_3}^{N_0} (1-2m_{n,z})^{i_1} (1+2m_{n,z})^{N-i_1}$$
$$\times (1-2m_{n-1,z})^{i_2} (1+2m_{n-1,z})^{N_0-i_2} (1-2m_{n+1,z})^{i_3} (1+2m_{n+1,z})^{N_0-i_3}$$
$$\times g\,[y_n, \Omega_n] \tag{A.14}$$

$$B_L = \frac{1}{2^{N+2N_0}} \sum_{i_1=0}^{N} \sum_{i_2=0}^{N_0} \sum_{i_3=0}^{N_0} C_{i_1}^{N} C_{i_2}^{N_0} C_{i_3}^{N_0} (1-2m_{L,z})^{i_1} (1+2m_{L,z})^{N-i_1}$$
$$\times (1-2m_{1,z})^{i_2} (1+2m_{1,z})^{N_0-i_2} (1-2m_{L-1,z})^{i_3} (1+2m_{L-1,z})^{N_0-i_3}$$
$$\times g\left[\frac{1}{2}(J_{\mathrm{I}}(N-2i_1) + J_{\mathrm{I}}(N_0-2i_2) + J_{\mathrm{I}}(N_0-2i_3)), \Omega_{\mathrm{I}}\right] \tag{A.15}$$

where

$$y_n = \frac{1}{2}\left[J_{n,n}(N-2i_1) + J_{n,n-1}(N_0-2i_2) + J_{n,n+1}(N_0-2i_3)\right] \tag{A.16}$$

and

$$g[y,\Omega] = \left.\frac{\partial f(y,\Omega)}{\partial h}\right|_{h=0}$$
$$= \frac{1}{2}\left\{\frac{\Omega^2}{(y^2+\Omega^2)^{3/2}} \tanh\left[\frac{1}{2}\beta(y^2+\Omega^2)^{1/2}\right]\right.$$
$$\left. + \frac{\beta}{2}\frac{y^2}{(y^2+\Omega^2)}\left\{1-\tanh^2\left[\frac{1}{2}\beta(y^2+\Omega^2)^{1/2}\right]\right\}\right\}. \tag{A.17}$$

## References


[1] Scott J F and Pazde Araiyo C A 1989 *Science* **246** 1400
[2] Moazzami R and Hu C 1992 *IEEE Trans. Electron Devices* **39** 2044
[3] Zhu W, Liu Z Q, Tse M S, Tan H S and Yao X 1996 *J. Appl. Phys.* **79** 4283
[4] Jaffe B, Cook W R Jr and Jaffe H 1971 *Piezoelectric Ceramics* (New York: Academic)
[5] Setter N and Collar E L (ed) 1993 *Ferroelectric Ceramics: Tutorial Review, Theory, Processing, and Applications* (Basel: Birkhauser)
[6] Herbert J M 1980 *Ferroelectric Transducers and Sensors* (New York: Gordon and Breach)
[7] Hwang C S, Park S O, Cho H J, Kang C S, Lee S I and Lee M Y 1995 *Appl. Phys. Lett.* **67** 2819
[8] Ichinose N and Ogiwara T 1997 *Ferroelectrics* **196** 9
[9] Tsai M S, Sun S C and Tseng T Y 1997 *J. Appl. Phys.* **82** 3482
[10] Camley R E and Stamps R L 1993 *J. Phys.: Condens. Matter* **5** 3727

[11] Lijima K, Terashima T, Bando Y, Kanigaki K and Terauchi H 1992 *Japan. J. Appl. Phys.* **72** 2840
[12] Tsurumi T, Suzuki T, Yamane M and Daimen M 1994 *Japan. J. Appl. Phys.* **33** 5192
[13] Wiener-Avnear E 1994 *Appl. Phys. Lett.* **65** 1784
[14] Tabata H, Tanaka H and Kawai T 1994 *Appl. Phys. Lett.* **65** 1970
[15] Kanno I, Hayashi S, Takayama R and Hirao T 1996 *Appl. Phys. Lett.* **68** 328
[16] Tilley D R 1988 *Solid State Commun.* **65** 657
[17] Schwenk D, Fishman F and Schwabl F 1988 *Phys. Rev.* B **38** 11 618
[18] Schwenk D, Fishman F and Schwabl F 1990 *J. Phys.: Condens. Matter* **2** 5409
[19] Schwenk D, Fishman F and Schwabl F 1990 *Ferroelectrics* **104** 349
[20] Qu B D, Zhong W L and Zhang P L 1994 *Phys. Lett.* A **189** 419
[21] Qu B D, Zhong W L and Zhang P L 1995 *Japan. J. Appl. Phys.* **34** 4114
[22] Wang C L and Smith S R P 1998 *J. Korean Phys. Soc.* **32** S382
[23] Wang C L, Zhong W L and Zhang P L 1992 *J. Phys.: Condens. Matter* **3** 4743
[24] Laaboudi B, Saber M, Benaboud A and Kerouad M 1999 *Acta Phys. Sin.* **8** 1004
[25] El Aouad N, Ainane A, Dujardin F, Kerouad M, Saber M and Stébé B 2000 *J. Magn. Magn. Mater.* **210** 366
[26] El Aouad N, Laaboudi B, Kerouad M, Saber M and Benaboud A 2000 *Chin. J. Phys* **38** 864
[27] El Aouad N, Laaboudi B, Kerouad M and Saber M 2000 *Phys. Status Solidi* b **221** 737
[28] Saber A, Essaoudi I, Ainane A and Saber M 1998 *Phys. Status Solidi* b **209** 161
[29] Saber A, Ainane A, Saber M, Essaoudi I, Dujardin F and Stébé B 1999 *Phys. Rev.* B **60** 4149
[30] Saber M 1997 *Chin. J. Phys.* **35** 577
[31] Tucker J W, Saber M and Peliti L 1994 *Physica* A **206**
[32] Hemberger J, Lunkenheimer P, Viana R, Böhmer R and Loidl A 1995 *Phys. Rev.* B **52** 1315
[33] Wang C L, Smith S R P and Tilley D R 1994 *J. Phys.: Condens. Matter* **6** 9633
[34] Torii K, Kaga T, Kushida K, Takeuchi H and Takeda E 1991 *Japan. J. Appl. Phys.* **30** 3562
[35] Hamada Y 1980 *Oyobutsuri* **49** 783
[36] Panitz J K 1979 *J. Vac. Sci. Technol.* **16** 315
[37] Srenivas K, Mansingh A and Sayer M 1987 *J. Appl. Phys.* **62** 4475
[38] Roy D and Krupanidi S B 1993 *Appl. Phys. Lett.* **62** 1056
[39] Kamalasanan M N, Kumar N P and Chandra S 1993 *J. Appl. Phys.* 5679